Theor Chem Acc (2012) 131:1072
DOI 10.1007/s00214-011-1072-z

REGULAR ARTICLE

Dynamics of collisions of hydroxyl radicals with fluorinated self-assembled monolayers

Diego Troya

Received: 7 June 2011 / Accepted: 5 August 2011 / Published online: 11 January 2012

Abstract We present a classical trajectory study of the dynamics of collisions between OH radicals and fluorinated self-assembled monolayers (F-SAMs). The gas/surface interaction potential required in the simulations has been derived from high-level ab initio calculations (focal-point-CCSD(T)/aug-cc-pVQZ) of various approaches of OH to a model fluorinated alkane. The two lowest-energy doublet potential energy surfaces considered in the electronic structure calculations have been averaged to produce a pairwise analytic potential. This analytic potential has been subsequently employed to propagate classical trajectories of collisions between OH and F-SAMs at initial conditions relevant to recent experiments on related systems. The calculated rotational distributions of the inelastically scattered OH agree well with the experiment, which serves to validate the accuracy of the simulations. Investigation of the dynamics of energy transfer for different initial rotational states of OH indicates that an increase in the initial rotation of OH results in increases in both the final average OH rotational and translational energy and in a slight decrease in the amount of energy transferred to the surface. Analysis of the dynamics as a function of the desorption angle of OH from the surface shows that while there is a correlation between the final scattering angle and OH's amount of final translational energy, the amount of rotational energy in OH is largely independent of the desorption angle. The mechanism of the collisions is found to be mostly direct; in about 90% of most trajectories, OH only collides with the surface once before desorbing, which exemplifies the rigidity of fluorinated monolayer surfaces and their inability to efficiently accommodate gas species.

Keywords Gas/surface scattering · Trajectory calculations · Intermolecular potentials · Self-assembled monolayers

1 Introduction

There is a growing interest in determining the outcome of collisions of gases with organic surfaces, as these heterogeneous processes play an important role in a variety of fields. In the environment, our understanding of the rich and complex chemistry involving aerosols [1] is further challenged because organics present at the surface of tropospheric particles [2] might play a role in the transport of matter in and out of the particles. Additional challenges to our understanding of gas/surface chemistry in the environment emerge by the continuous processing of aerosol surface organics by gas-phase oxidizers [3], of which the hydroxyl radical is the most abundant [4].

A convenient way to perform systematic studies of the reactions of common atmospheric oxidizers with organic matter in the laboratory is to immobilize the latter in solid supports using self assembly on metal surfaces [5]. Employing self-assembled monolayer technology, D'Andrea et al. [6] have recently investigated the reactions of OH radicals with alkane- and alkene-thiol molecules absorbed on gold. Using a similar setup, Fiegland et al. [7] have studied the degradation of vinyl-terminated alkanethiol self-assembled monolayers (SAMs) by gas-phase ozone.

A technical disadvantage to the use of SAMs in the experiment to examine the degradation of organic material

Published as part of the special collection of articles celebrating the 50th anniversary of Theoretical Chemistry Accounts/Theoretica Chimica Acta.

D. Troya (✉)
Department of Chemistry, Virginia Tech,
107 Davidson Hall, Blacksburg, VA 24061-0212, USA
e-mail: troya@vt.edu

by common oxidizers is that the surface is constantly changing as reactions take place, and this makes it difficult to obtain atomistic information about the reaction mechanisms. Complementary experimental setups that avoid this problem are therefore rather valuable. An alternative and convenient way to perform detailed studies of the processing of organic surfaces by atmospheric oxidizers is to employ continually refreshed organic liquids of well-controlled composition. Indeed, the field of experimental gas/liquid reaction dynamics has advanced greatly in recent time, from the proton-exchange studies by Nathanson [8] and the reactions of O atoms with squalane [9] and room-temperature ionic liquids (RTILs) [10] by Minton (both using time-of-flight detection of products), to the studies of F-atom + squalane reactions by Nesbitt [11], and O-atom reactions with squalane [12] and RTILs [13] by McKendrick (both using spectroscopic detection of products). Using a gas/liquid experimental setup, the latter group has recently investigated the inelastic dynamics and reactions OH with a variety of organic liquids [14, 15]. These experiments on OH scattering from liquids have provided motivation for the simulations presented in this paper.

A common pursuit of these detailed gas/surface experiments is to unveil the factors that control whether a gas traps on a surface or recoils promptly into the gas phase after collision. Obtaining the sticking probability is important because most gas/surface reactions with appreciable barrier to reaction are thought to proceed via a Langmuir–Hinshelwood mechanism whereby gases thermally accommodate on a surface prior to reaction. Advances in detailed molecular dynamics simulations have proved useful in helping to elucidate the microscopic details of gas/surface collisions involving organics. Initial simulation efforts were devoted to rare gas scattering, with SAMs acting as the organic surface of choice because they are generally more convenient to use in the calculations than liquid surfaces [16–18]. More recent theoretical work has progressed to molecular scattering from surfaces with state-to-state resolution, with examples including CO_2 [19], CO [20], and HCl [21] scattering from SAMs having various functionalities at the gas/solid interface.

In this work, we begin a study of the dynamics of collisions of important atmospheric oxidizers with organic surfaces by investigating the inelastic scattering of OH from fluorinated self-assembled monolayers (F-SAMs). As mentioned before, this work is motivated recent experiments by the McKendrick group [14, 15] and by the necessity of fully understanding heterogeneous processes in the environment involving organics. A significant complication of this study compared to the prior work reviewed above is that the gas-phase collider is an open-shell species. While the surface chosen in this work is inert, and therefore, the potential energy surfaces governing the dynamics are non-reactive, the $^2\Pi$ nature of OH's ground state implies participation of two surfaces in the collisions, which introduces new challenges in the simulations.

The reminder of this paper is as follows. In Sect. 2, we describe the electronic structure calculations and fit of the potential energy surfaces required to simulate collisions of OH with fluorinated surfaces. In Sect. 3, we present a classical trajectory study of OH collisions with F-SAMs aimed at shedding light into recent experiments. Finally, we offer some concluding remarks in Sect. 4.

2 Potential energy surfaces

In order to carry out reliable classical dynamics studies of gas/surface collisions, the potential energy and its gradients with respect to atomic positions need to be accurately known. The potential energy surface of a standard gas/surface system can be generally divided into three components: the potential energy surface corresponding to the organic surface, that of the gas species, and the one responsible for the interactions between the gas and the surface.

Traditionally, organic surfaces have been represented by standard force fields such as OPLS [22] or MM3 [23], as these force fields bear out the essential properties of the surfaces. MM3 has been used to describe the surface potential in this work.

Regarding the gas species, in this work, we have represented the diatomic potential energy of the hydroxyl radical by a Morse potential:

$$V_{\mathrm{OH}} = D\left[1 - \mathrm{e}^{-\beta(r-r_{\mathrm{e}})}\right]^2 \qquad (1)$$

with $D = 101.4$ kcal/mol, $\beta = 2.353$ Å^{-1}, and $r_{\mathrm{e}} = 0.9696$ Å. This set of parameters provides spectroscopic constants for OH in excellent agreement with experiment. For instance, the calculated vibration frequency is 3,737 cm^{-1} (3,738 cm^{-1} experimentally [24]) and the rotational constant is 18.91 cm^{-1} (18.91 cm^{-1} experimentally [24]).

Regarding the gas/surface potential, prior work has shown that the non-bonding terms of standard force fields are generally not sufficiently accurate for use in detailed scattering simulations [25]. Therefore, in this work, we have derived our own analytic potential to describe the interaction between the hydroxyl radical and a fluorinated surface. The strategy used to derive this potential is based on the assumption that the interaction between the atoms of a gas species approaching a surface and those of the surface are pairwise and additive. This strategy has been employed before in a number of simulations of gas/surface collisions with excellent results [17, 19, 20]. The pairwise potentials are obtained from a fit to ab initio calculations on relevant

regions of the entire potential energy surface of the system. In the rest of this section, we describe the ab initio calculations carried out to accurately map the potential for hydroxyl radicals interacting with fluorinated species and the fit of an analytical potential to those ab initio data.

2.1 Ab initio calculations

To determine the intermolecular interactions of OH with fluorinated alkanes, we have computed the potential energy of various approaches of OH to the simplest perfluoroalkane, CF_4. The selected approaches of OH to CF_4 are inspired by prior work on the development of gas/surface potentials using rare gases [26] or symmetric molecules such as CO_2 [19]. However, there are two noteworthy differences with respect to that prior work. First, the OH molecule is not symmetric about its center, and this implies that approaches in which the H-end or O-end of the molecule face the fluoroalkane molecule both need to be explicitly considered. Operationally, this means that the sampling of potential energy surface has been significantly more costly than in prior work. Figure 1 shows the 12 approaches whose potential energy we have computed using ab initio methods denoted by the labels that will be used hereafter to identify them. (Note that in prior work with rare gases or symmetric molecules, only 2 or 3 approaches were typically considered [19, 26].)

In approaches a and b, OH nears CF_4 so that the OH internuclear axis is perpendicular to one of the faces of the CF_4 tetrahedron. Approaches c and d are similar, but OH and the closest vertex of the CF_4 tetrahedron are collinear. The OH internuclear axis is perpendicular to a CF_4 tetrahedron edge in approaches e and f. The rest of the approaches are designed to capture situations in which neither the H- nor the O-end of the hydroxyl radical approaches CF_4 more prominently than the other end. Thus, in these approaches, the OH bond is parallel to the face of the CF_4 tetrahedron (g and h), perpendicular to the closest C–F bond (i and j), and perpendicular to both the bisector of the closest F–C–F angle and a CF_4 tetrahedron edge (k and l).

The potential energy along each of the approaches in Fig. 1 has been computed at the MP2/aug-cc-pVQZ level of ab initio theory. To add a further level of electronic correlation to these ab initio calculations, the CCSD(T) energy with that basis set has been estimated via the focal-point approximation [27]. The focal-point approximation is based on the observation that the difference between MP2 and CCSD(T) energies for each point of a potential energy surface is constant regardless of the basis set and has been shown to perform superbly for intermolecular interactions of the type investigated in this work [26]. Thus, by computing the difference between CCSD(T) and MP2 energies for all of the points of the approaches in Fig. 1 with the aug-cc-pVDZ basis set, one can conveniently estimate CCSD(T)/aug-cc-pVQZ energies from MP2/aug-cc-pVQZ calculations. Hereafter, we will refer to the estimated CCSD(T) energy using the focal-point approximation as fp-CCSD(T). All electronic structure calculations in this work have been computed using the Gaussian 09 package of programs.

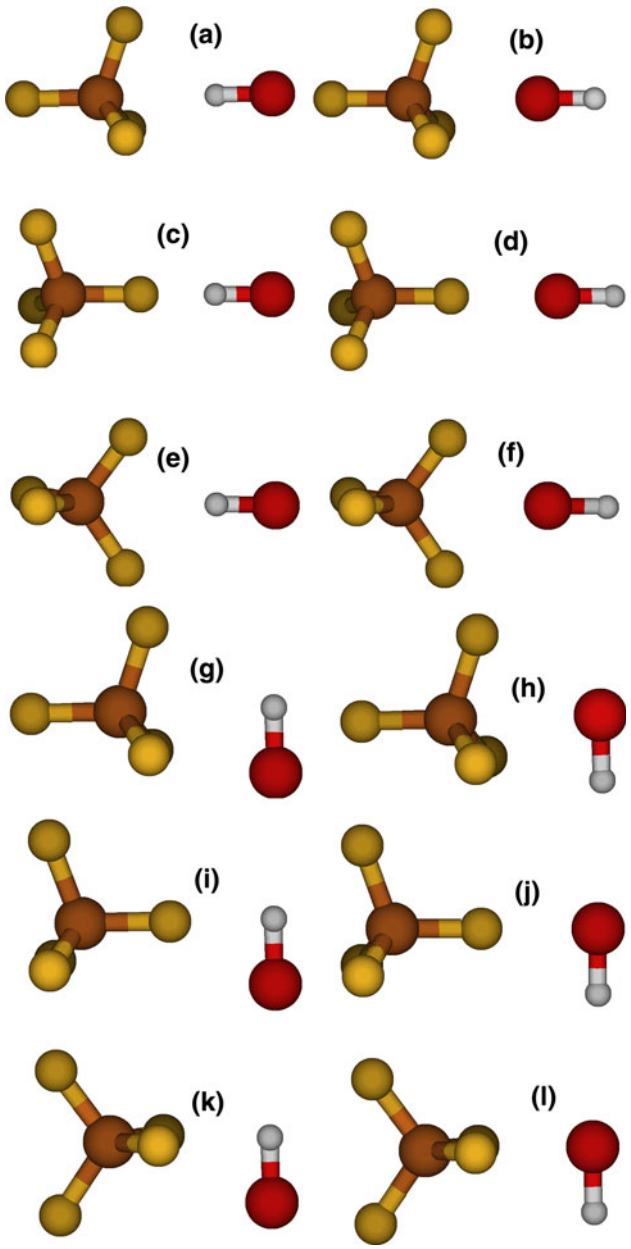

Fig. 1 Approaches of OH to CF_4 explored with ab initio calculations in this work

A second major difference between the ab initio calculations aimed at mapping the gas/surface potential in this work and those in prior efforts is in the open-shell nature of the OH radical. The two components of the $OH(^2\Pi)$ state give rise to two different potential energy surfaces that can be

accessed during the interaction with a closed-shell colliding partner. While some of the approaches in Fig. 1 have higher point-group symmetries than C_s (approaches a–d are nominally C_{3v}), all of the calculations have been carried out in C_s point-group symmetry, and the two potential energy surfaces emerging from the interaction of OH with CF_4 are thus of A′ and A″ symmetry. To accurately consider the interaction of OH with fluorinated alkanes, we have therefore needed to carry out calculations on both A′ and A″ potential energy surfaces for each of the approaches in Fig. 1, which significantly increases the computational expense.

Each potential energy surface has been scanned for each approach from the asymptote until repulsive energies of about 30 kcal/mol. The geometries of the OH and CF_4 molecules have been held frozen at their respective minimum energy values, and the coordinate that connects the C atom of CF_4 and the closest of the atoms in OH has been scanned at 0.05 Å steps. Approximately, 50 points have been computed per approach and potential energy surface. Overall, 1,224 ab initio points have been calculated in this work at the fp-CCSD(T)/aug-cc-pVQZ level to map the A′ and A″ potential energy surfaces responsible for the interaction between OH and CF_4.

Figure 2 presents the potential energy profiles of all of the scans that we have calculated in this work for both the A′ and A″ surfaces distributed among the same approaches as depicted in Fig. 1. Only energies of up to 5 kcal/mol are shown in the figure so that the differences at the minima can be appreciated. The energy curves have the expected profile of a weakly attractive potential well at long distances and a repulsive wall at shorter intermolecular separations. The A′ and A″ surfaces are essentially degenerate for the approaches of nominal C_{3v} geometry (a–d). In the rest of approaches, the A″ surface is always more repulsive than the A′ surface except for the g and h approaches, in which the well is slightly deeper for the A″ surfaces, even if the wall is more repulsive for this surface too. This rather nuanced behavior of the A′ and A″ surfaces draws attention to the fact that one cannot estimate one surface from the other in a straightforward manner; instead, both surfaces must be computed explicitly.

Table 1 lists the location and energy of the attractive well for each approach and surface, with which the trends emerging from Fig. 2 can be corroborated: except when degeneracy exists, the well in the A″ surface always appears at longer separation distances than in the A′ surface. In addition, the A″ wells are shallower than in the A′ surface, except for approaches g and h. An immediate conclusion of the data in Fig. 2 and Table 1 is that the attraction between OH and fluoralkanes is rather weak. Therefore, one can anticipate that if OH approaches a fluorinated surface at superthermal energies, such as in the experiments of McKendrick and co-workers [14, 15], the probability for physisorption of OH on the surface leading to long residence times should not be very large. The mechanistic studies that we present in Sect. 3 will quantify the extent to which OH traps on the F-SAM surfaces or recoils after a brief interaction.

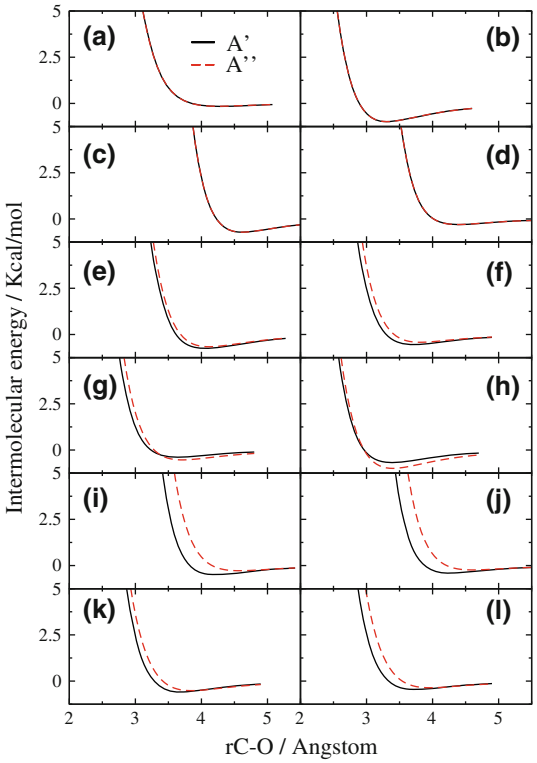

Fig. 2 Intermolecular potential energy of approaches of OH to the CF_4 molecule as a function of the distance between the O and C atoms calculated at the fp-CCSD(T)/aug-cc-pVQZ. **a–l** Correspond to the approaches in Fig. 1

In the following section, we describe how we have used these ab initio data to obtain an analytic potential for use in chemical dynamics simulations.

2.2 Fit of analytic potentials

To enlist the high-level electronic structure calculations described before in classical trajectory simulations of OH + F-SAM collisions, we have derived analytical potentials directly from the ab initio data. In this work, the intermolecular potential of an atom in a fluoroalkane molecule interacting with one of the OH atoms is represented by a Buckingham function:

$$V_{ij} = A_{ij} e^{-B_{ij} r_{ij}} + \frac{C_{ij}}{r_{ij}^6} \quad (2)$$

in which the A, B, and C parameters are adjustable and specific to each pair of atoms, and r_{ij} is the distance between the atoms. In general, the exponential term is responsible for representing the repulsive part of the

Table 1 Energy and location and of the attractive well in approaches of OH to CF_4 in the A′, A″, and fitted surfaces

Approach	A′	A″	V_{sum} (fit)[a]
a	0.15 (4.23)	0.15 (4.23)	0.20 (4.28)
b	0.99 (3.30)	0.99 (3.30)	0.84 (3.40)
c	0.71 (4.61)	0.71 (4.61)	0.70 (4.56)
d	0.30 (4.38)	0.30 (4.38)	0.29 (4.58)
e	0.76 (4.03)	0.66 (4.13)	0.46 (4.13)
f	0.55 (3.70)	0.42 (3.80)	0.58 (3.80)
g	0.39 (3.63)	0.53 (3.73)	0.60 (3.63)
h	0.68 (3.35)	0.99 (3.40)	0.78 (3.45)
i	0.50 (4.19)	0.28 (4.58)	0.42 (4.39)
j	0.40 (4.28)	0.24 (4.63)	0.34 (4.48)
k	0.59 (3.68)	0.52 (3.83)	0.63 (3.78)
l	0.45 (3.75)	0.36 (3.95)	0.59 (3.80)

Energy is in kcal/mol below the asymptote. The values in parentheses correspond to the minimum energy C–O distance in Angstrom. For the A′ and A″ surfaces, the data are from fp-CCSD(T)/aug-cc-pVQZ calculations

[a] Data corresponding to the global analytic function. See text

potential, while the second term is expected to capture the attractive region (the C coefficient is thus generally negative). While an inverse sixth-power dependence of the attractive term on the separation distance is the traditional form of the potential because it has the same dependence on distance as van der Waals interactions, in some earlier work, the power of the distance has also been optimized for added flexibility [21]. In this work, we attempted to fit the ab initio data with both Eq. 2 and letting the exponent in the second term vary. The latter approach did not offer a dramatic improvement in the fit, and we thus chose to use the traditional Buckingham potential in Eq. 2 for simplicity.

Since two potential energy surfaces intervene in the dynamics of collisions of OH with an F-SAM, an important question is how to combine these surfaces to be able to compute dynamics properties that can be compared directly to experiment. The formalism of the combination was developed by Alexander in the 1980s for an open-shell diatomic molecule colliding with a structureless closed-shell species [28]. For a $^2\Pi$ molecule captured by Hund's case (a), state-to-state calculations that aim at reproducing experimental transitions in a given spin–orbit manifold require use of the V_{sum} potential, which is the straight average of the A′ and A″ surfaces. The V_{dif} potential, which is the half the difference between the two surfaces, is responsible for transitions between different spin–orbit manifolds. This formalism for Hund's case (a) has commonly been applied to quantum dynamics calculations of inelastic scattering of OH($^2\Pi$) from rare gases [29]. Since in this work the nuclear dynamics is purely classical, the fine structure of the rotating OH radical (both the Λ doubling and spin–orbit states) is entirely neglected, and all calculations are carried out with the V_{sum} potential. Therefore, our study will primarily capture the dynamics of collisions that conserve the spin–orbit state of OH in the experiment, as has been the norm in classical trajectory simulations of energy transfer involving open-shell species in the gas phase [30].

Table 2 Parameters of the pairwise Buckingham potential fitted to V_{sum} fp-CCSD(T)/aug-cc-pVQZ ab initio points

Pair	A_{ij} (kcal/mol)	B_{ij} (Å^{-1})	C_{ij} (kcal Å^6/mol)
O–F	34,616	3.6736	−409.55
O–C	36,328	3.8348	−876.52
H–F	19,827	4.5130	−209.58
H–C	−66,879	4.6535	1,127.3

To derive an analytical expression for the V_{sum} potential, we have averaged the energies of each calculated point on the A′ and A″ surface at the fp-CCSD(T)/aug-cc-pVQZ level and fitted them using the Buckingham potential of Eq. 2. A non-linear least-squares parameter optimization is utilized to obtain the parameters A, B, C of each pair of atoms (O–F, O–C, H–F, and H–C) that best fit the ab initio data. These pair-specific parameters are listed in Table 2. In the fit, the parameters were not restrained so that the exponential term is repulsive and the polynomial term is attractive, and for the H–C pair, the signs of the A and C parameters are negative and positive, respectively, which is not the norm, but provides the best fit to the electronic structure points. In fact, the analytic function fits the ab initio data well, with a global root-mean-square deviation of 0.11 kcal/mol in the attractive region of the potential and of 0.47 kcal/mol for all points up to repulsive energies of 30 kcal/mol. More quantitative information of the fitted surface can be obtained from Table 1, where we show the location and energy of the minima along all of the approaches in the fitted V_{sum} potential. In the next section, we describe how we have employed this analytic potential to propagate trajectories of collisions of OH with a fluorinated surface and compare our results with recent experimental measurements.

3 Classical trajectory calculations

To simulate recent experiments on the inelastic scattering of OH from fluorinated alkane surfaces, we have computed the dynamics of collisions of OH from a semifluorinated alkanethiol self-assembled monolayer via classical trajectories. While the experiments considered the scattering of OH from perfluoropolyether (PFPE, a liquid at ambient conditions) [14, 15], extensive theoretical and experimental

work on the scattering of CO_2 from that liquid and F-SAMs has nicely shown that both surfaces are comparable [19, 31].

The F-SAM surface is composed of 25 S–$(CH_2)_2$–$(CF_2)_5$–CF_3 chains arranged in the pattern they adopt on a Au(111) surface [32]. Periodic boundary conditions are used to replicate the unit cell formed by the 25 chains and simulate an extended surface. Our choice of a semifluorinated surface instead of a fully fluorinated surface is motivated by the commercial availability of the former. However, we note that the presence of non-fluorinated methylene groups in the unexposed region of the SAM should be irrelevant to the work presented here, because not a single trajectory exhibits deep penetration of OH into the surface. The separation between the semifluorinated chains in the SAM is either 4.98 or 5.77 Å. 4.98 Å corresponds to the chain separation in non-fluorinated SAMs [32], while 5.77 Å has been measured for semifluorinated SAMs [33].The bulk densities of these surfaces are 2.5 and 1.8 g/cm^3, respectively, with the density of only the fluorinated part being approximately 15% higher. The bulk density of the liquid used in the experiments is 1.9 g/cm^3. As we show below, density seems to play a minor role in the dynamics of OH collisions with fluorinated surfaces at low energy.

To generate initial coordinates and momenta for the surface atoms, we have performed a 2 ns canonical (constant temperature and volume) simulation of only the SAM at 300 K. During the last 0.5 ns of this simulation, intermediate coordinates and momenta are saved every 500 fs for use as initial conditions for the surface in collisions with OH.

Regarding the initial conditions for the gas species, the OH used in the experiment emerges from photolysis of HONO at 355 nm [14]. The resulting kinetic-energy distribution of the OH radical is relatively narrow and peaks at 12.8 kcal/mol. All of the calculations in this work therefore correspond to that collision energy (E_{coll}). The photo-induced OH radical is vibrationally cold, but has substantial rotational population up to $N = 7$ states. In the calculations of this work, the OH is initially in the ground vibrational state ($v = 0$), and various initial rotational states are probed. While the experiments measure the total angular momentum N of OH (exclusive of electron spin), in our classical dynamics calculations, we only access the nuclear rotational angular momentum J. To establish a correspondence between both, we use $N = J + 1$, which is a correct mapping for low levels of rotational excitation [34].

A final consideration on the initial conditions of the classical trajectories pertains to the angle of incidence formed by the initial velocity vector of OH and the surface normal. In the photolysis experiments [14], OH is generated in all directions of space. However, the laser-induced fluorescence detection is most sensitive to OH that collides normal to the surface. Therefore, all of our simulations consider normal incidence.

The OH molecule is placed initially at least 10 Å from the closest atom in the surface, and the trajectories are propagated until the recoiling OH reaches a distance of at least 10 Å from the closest surface atom after collision. The impact point on the surface is randomly sampled from a plane that represents the unit cell of the SAM. Batches of 3,000 trajectories per initial set of OH rovibrational states have been computed. To calculate the rotational state of OH after collision, the components of the rotational angular momentum (J_x, J_y, and J_z) are obtained from the cross product of the final diatomic position and momentum vectors, and the rotational quantum number is the nearest integer of the quantity $J = \sqrt{J_x^2 + J_y^2 + J_z^2} - 0.5$. To compare with the experiment, we assign $N = J + 1$, as explained before.

3.1 Influence of surface density

As mentioned before, we have considered two SAM surfaces with interchain separations of either 4.98 or 5.77 Å. Prior experimental [35] and theoretical [17] work has showed that in the case of high-energy (19.1 kcal/mol) Ar scattering from regular hydrogenated alkanethiol SAMs, the surface density plays a notable role on the amount of gas/surface energy transfer. More dense surfaces represent SAMs in which the chains are packed more tightly and thus have more difficulty in dissipating energy transferred upon gas impingement.

To verify the effect of surface density in collisions of OH with F-SAMs at conditions relevant to the experiment, we have analyzed 3,000 trajectories with OH in its ground rovibrational state impinging on the surfaces with normal incidence at $E_{\mathrm{coll}} = 12.8$ kcal/mol. Remarkably, the properties of OH recoiling from both F-SAMs are nearly indistinguishable. The average final OH translational energy ($\langle E'_{\mathrm{T}} \rangle$) in both simulations is 4.5 kcal/mol, which represents a translational energy transfer efficiency of $(E_{\mathrm{coll}} - \langle E'_{\mathrm{T}} \rangle)/E_{\mathrm{coll}} = 0.65$. OH does not gain essentially any vibrational excitation upon collision with either surface (the change in vibrational energy upon collision is less than 2% of the zero-point energy under all conditions examined), and its average rotational energy is 0.4 kcal/mol in the less dense surface, and 0.3 kcal/mol in the surface with an interchain spacing of 4.98 Å. Figure 3 shows the full rotational distributions obtained in the simulations with both surfaces, where the slight excess of rotational energy in the low-density surface anticipated in the average rotational energies can be appreciated.

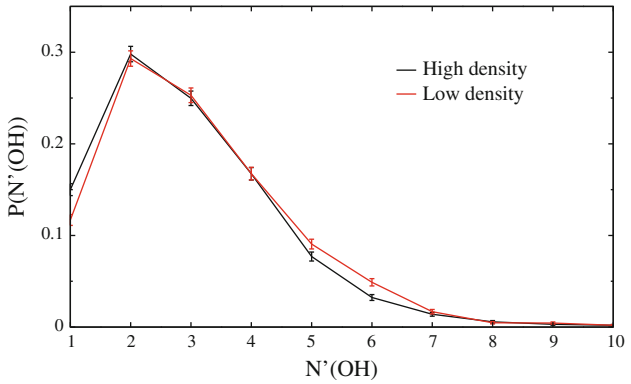

Fig. 3 OH rotational distributions obtained in collisions of OH with fluorinated SAM surfaces at $E_{coll} = 12.8$ kcal/mol and normal incidence. The low-density SAM surface corresponds to an interchain separation of 5.77 Å and the high-density surface to 4.98 Å

The fact that the amount of energy absorbed by both F-SAM surfaces is essentially the same in the simulations is in contrast with the work on Ar scattering from regular hydrogenated surfaces of different densities mentioned above. Leaving dissimilitudes in the potential energy surfaces aside, there are two main differences that can be responsible for the OH + F-SAM collisions dynamics in this work not following the Ar + H-SAM results. First, the rare gas scattering studies were performed at collision energies slightly higher than those in this work (19.1 kcal/mol vs. 12.8 kcal/mol). Second, there is an obvious mismatch in the masses of the gas (40 amu vs. 19 amu) and surface atoms (CH_3- vs. CF_3-termini). Studies of the influence of collision kinematics on energy exchange in gas/SAM collisions indicate that surfaces with rather different masses behave similarly if the momentum of the impinging gas is not large enough to induce significant lateral motion of the SAM chains [18]. Since OH is approximately twice lighter than Ar, and its collision energy in this work is lower than that of Ar in the prior work, its momentum might not be sufficient to induce significant lateral motion of a heavy fluorinated SAM chain, regardless of the SAM packing density. This inability of OH to transfer enough momentum to the surface so that the inertial barrier for chain motion can be overcome explains the insensitivity of translational energy transfer to surface density.

In search for an explanation to the slightly enhanced OH rotation when colliding with a lower density surface, we note that the larger separation between chains in the lower density SAM makes it slightly more corrugated than the tighter-packed higher density SAM. This microscopic corrugation might elicit larger torques to an impinging OH molecule, which could result in enhanced rotational excitation. Since the scattering results at the initial conditions of this work are largely insensitive to the surface density, all of the subsequent simulations have been performed with only the F-SAM that has an interchain separation of 4.98 Å.

As mentioned before, a complication of the current work is in the involvement of two potential energy surfaces in the scattering process. To characterize the effect of using only one of these surfaces or the V_{sum} potential, we have computed trajectories for the surface of lower density with a potential obtained by fitting the data coming only from the $^2A'$ state (1^2A in C_1 symmetry). The trajectories have used the same initial conditions as for the surface density studies just presented ($E_{coll} = 12.8$ kcal/mol, OH in ground rovibrational state, normal incidence). The average final translational energy of OH obtained with the 1^2A surface (5.70 kcal/mol) is significantly larger than with the V_{sum} potential (4.48 kcal/mol). The average final rotational energy is not so largely affected by the choice of surface (0.29 kcal/mol vs. 0.32 kcal/mol, respectively for the 1^2A and V_{sum} surfaces), but other scattering properties are also noticeably influenced by the surface. For instance, the average desorption angle with respect to the surface normal (36.4 and 41.6° with the 1^2A and V_{sum} surfaces, respectively) shows deviations between the two potentials that, as we shall see below, are larger than between different initial rotational states of OH using the V_{sum} surface. The conclusion of this investigation is that for the system under study, calculating the dynamics with only one surface provides results that differ significantly from the average of the two surfaces involved. Using the average potential is the common strategy in gas-phase studies, and thus, all of the results presented hereafter refer to the V_{sum} potential.

3.2 Energy transfer

We now turn our attention to characterizing how the properties of the recoiling OH depend on its initial rotational state. The importance of this study resides on the fact that in the experiments of the McKendrick group, OH strikes a fluorinated surface having a distribution of initial rotational energies [14]. Thus, the product energy distributions emerge from the contributions of trajectories started with various OH initial rotational states. Figure 4 displays final OH rotational distributions for collisions at $E_{coll} = 12.8$ kcal/mol, normal incidence, and initial OH rotational states $N = 1$, 3, 5, and 7. Clearly, there is a correlation between the level of initial rotational excitation and product rotation. For ground-state OH, $N = 1$, there is a substantial gain of rotational excitation during the collision, which indicates that some of the collision energy is channeled into product OH rotation ($T \rightarrow R'$ energy transfer). The rest of the initial collision energy is retained by OH as final translational energy or is absorbed by the surface (as mentioned above, the collisions are

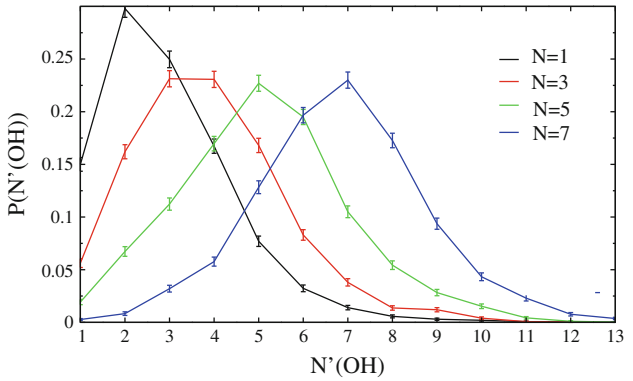

Fig. 4 OH rotational distributions obtained in collisions of OH with fluorinated SAM surfaces at $E_{coll} = 12.8$ kcal/mol and normal incidence for various initial rotational states of OH

Table 3 Average final translational and rotational energy of OH after collisions with a fluorinated surface

Initial OH state	E_R	$\langle E'_R \rangle$	$\langle E'_T \rangle$	$\langle \Delta E_{surf} \rangle$
$N = 1$	0	0.32	4.48	8.00
$N = 3$	0.20	0.58	4.55	7.87
$N = 5$	0.83	1.09	4.77	7.77
$N = 7$	1.89	1.98	4.99	7.72

All energies in kcal/mol, error bars are approximately 1%

vibrationally adiabatic). For OH initially rotationally excited, collisions with the fluorinated surface result in either a loss or a gain of initial rotational energy, as OH rotational states lower and higher than the initial one become populated. Average final rotational energies ($\langle E'_R \rangle$) are presented in Table 3 as a function of the initial rotational state. Those data show that for the rotational levels explored in this work, there is always a net gain of rotational energy upon collision. However, the net gain is rather small and decreases with larger initial rotational excitation.

Figure 5 presents a comparison between the final OH rotational distributions calculated in this work and the ones measured in the experiment [14]. In order to produce simulation results that can be compared with experiment, the rotational distributions generated in calculations in which OH initially possesses rotational states $N = 1$–7 are weighted by the rotational populations measured immediately after photolysis in the experiment. The laser-induced fluorescence experiments determined populations using the R_1, R_2, and Q_1 branches, and here, we present our calculated results in comparison with both the R_1 branch and the average of all measurements (obtained as $R_1 + R_2 + Q_1(R_1/R_2)$ as recommended by the experimentalists). The simulations reproduce experiment quite well, lending support to the techniques used in the calculations. There are several caveats

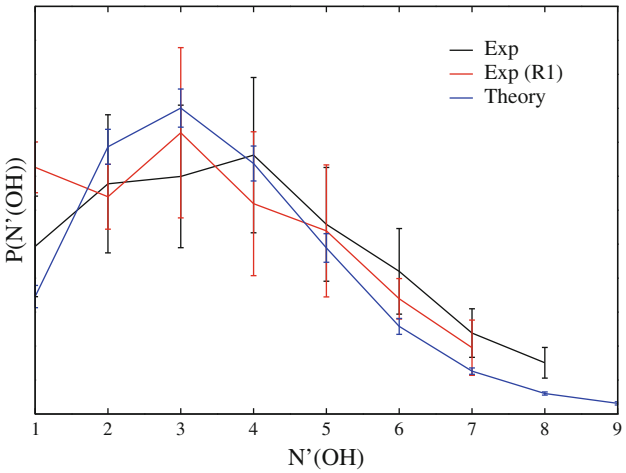

Fig. 5 OH rotational distributions obtained in collisions of OH with fluorinated SAM surfaces at $E_{coll} = 12.8$ kcal/mol and normal incidence. The experiments are from Ref. [14]. The calculated results have been obtained by averaging rotational distributions from specific initial rotational states of OH weighted by their photolytic populations (see text)

in the theory–experiment comparison exhibited in Fig. 5. First, the experiments correspond to scattering of OH from liquid PFPE, while the simulations are for an F-SAM. However, as discussed before, there is evidence supporting the resemblance of these two surfaces toward scattering gases [19]. In addition, the comparison between surfaces of different densities introduced earlier in this paper further supports the notion that the details of the surface are perhaps not critical in this work. Second, the calculations have been performed with the V_{sum} potential, which is expected to capture rotational transitions within the same spin–orbit manifold. On the other hand, the experiments indicate that non-adiabatic dynamics is not negligible [14, 15], so not all of the flux measured in the experiment should in principle be reproduced by the calculations in this work. Finally, the initial conditions in the experiment are not as well defined as in the calculations. While the experiment is most sensitive to normal-incidence OH, contributions from other incident angles are possible but difficult to quantify experimentally. Notwithstanding the difficulties in establishing a quantitative comparison between theory and experiment, the emerging conclusion from Fig. 5 is that the potential energy surfaces derived in this work provide an at least reasonable description of experiment.

To complete our understanding of energy transfer in OH + F-SAM collisions, we now examine the amount of initial energy carried by OH as final translation and the amount of initial energy transferred to the surface. Table 3 lists the average final rotational and translational of OH, and the average amount of energy transferred to the surface as a function of the initial OH rotational state. Comparison of the initial and final translational and rotational energies

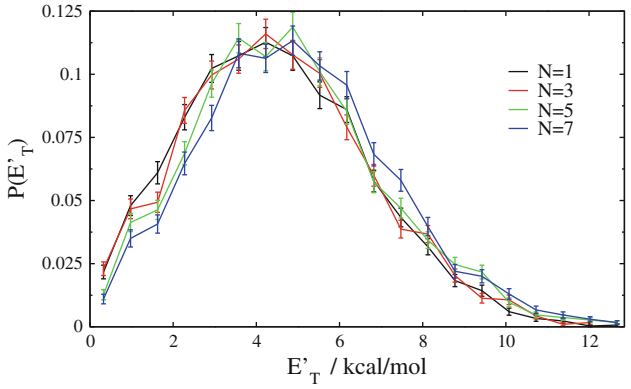

Fig. 6 OH product translational energy distributions obtained in collisions of OH with fluorinated SAM surfaces at $E_{coll} = 12.8$ kcal/mol and normal incidence for various initial rotational states of OH

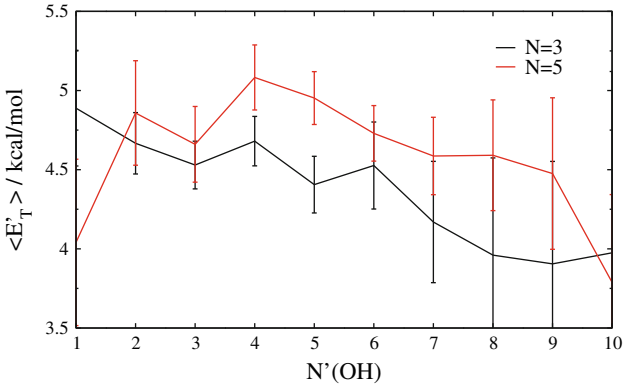

Fig. 7 OH final average translational energy as a function of the final OH rotational state in collisions of OH ($N = 3,5$) with fluorinated SAM surfaces at $E_{coll} = 12.8$ kcal/mol and normal incidence

clearly shows that most of the initial OH energy is lost to the surface, with a slight amount going to OH rotation. Interestingly, there is also a direct correlation between initial OH rotation and final OH translation, even if the increase of final translational energy with initial rotational energy is modest. Figure 6 displays the OH final translational energy distributions for various initial rotational states of OH, where the influence of initial OH rotation on the amount of energy retained by OH as translation after collision can be fully appreciated. This increase in final OH translational energy with increasing initial rotational excitation in OH, tied to the net gain in OH rotation upon collision, implies that there is less and less energy being transferred to the surface with increasing initial rotational excitation of OH. This trend can be substantiated by the average energy gain by the surface in Table 3 (ΔE_{surf}), which clearly shows how initial OH rotation acts to slightly inhibit energy transfer to the surface.

The examination of OH final rotational and translational energies in Figs. 4 and 6 reveals rather broad distributions. An interesting question then is to analyze whether trajectories in which OH is translationally hot also cause rotational excitation or whether rotational and translational modes compete for the energy available to the OH molecule during collision. The importance of this question is exacerbated by recent experimental [11] and theoretical [36] work on the *reactive* scattering of low-energy F atoms ($E_{coll} < 1$ kcal/mol) from alkane surfaces, where it was seen that HF products that result translationally excited are also rotationally excited. Figure 7 shows OH rotational-state-specific average final translational energies for two initial rotational states of OH. For OH initially in $N = 3$, in spite of the sizeable error bars, we see the absence of a positive correlation between final translation and rotation. On the contrary, there seems to be a somewhat faint decrease in the amount of final translational energy when OH becomes rotationally excited. This trend would seem to point toward the competition of rotational and translational degrees of freedom for available energy. For $N = 5$, an interesting phenomenon happens. We distinguish among three regimes of final OH rotation to facilitate discussion. First, OH that is rotationally cold after collision is also relatively translationally cold. This results implies when the surface efficiently absorbs OH rotational energy and quenches it significantly ($N = 5 \rightarrow N' = 1$), it also efficiently absorbs energy from OH initial translation. Second, collisions that are rotationally adiabatic or either gain or lose a modest amount of OH rotation ($N = 5 \rightarrow N' = 4$–6) show the largest amount of OH final translation. Finally, if OH gains substantial rotational energy during the collision ($N = 5 \rightarrow N' > 8$), it does not retain as much of its initial translational energy as when the collisions are rotationally adiabatic. These trends are significantly different from those seen in the highly exothermic HF-forming reactions of F atoms with condensed-phase alkanes, which highlights the wealth of dynamic routes that can come into play when a gas strikes an energy-absorbing organic surface, with which it might exchange energy, react, or both.

3.3 Angular distributions

While the experiments currently available for OH collisions with fluorinated surfaces are not exquisitely specific to the angle at which OH desorbs with respect to the surface normal, future use of molecular beam techniques with time-of-flight detection might furnish angular information about the recoiling OH. Figure 8 shows the distributions of the angle of desorption of OH (with respect to the surface normal, θ_f), for various initial rotational states of OH. The distributions are very broad and peaked in the 30°–45° range. A first conclusion of the study of desorption angles is that the scattering of OH from fluorinated surfaces is that instead or recoiling in the direction of impingement, a wide range of angles are accessed in the desorption process of

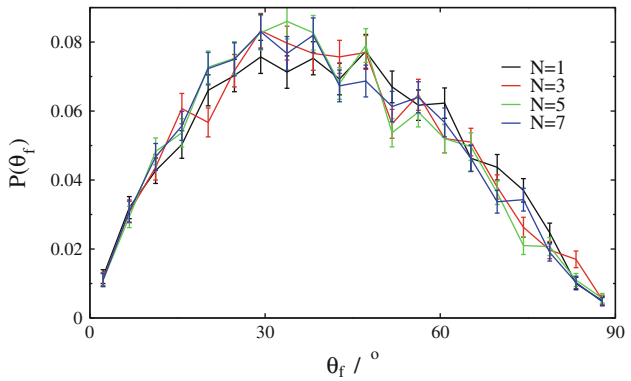

Fig. 8 OH final polar scattering angle distributions in collisions of OH with fluorinated SAM surfaces at $E_{coll} = 12.8$ kcal/mol and normal incidence for various initial rotational states of OH

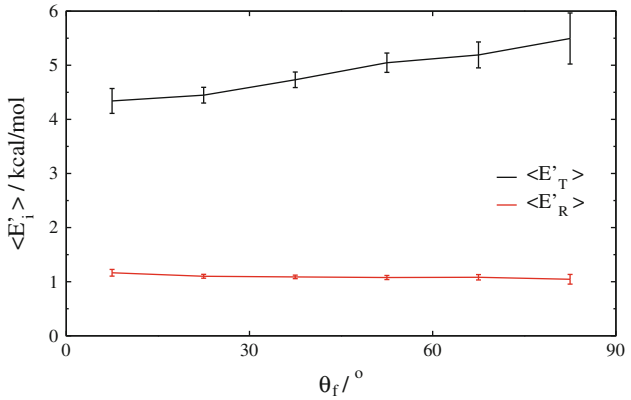

Fig. 9 OH final average translational and rotational energy as a function of the polar scattering angle distributions in collisions of OH ($N = 5$) with fluorinated SAM surfaces at $E_{coll} = 12.8$ kcal/mol and normal incidence

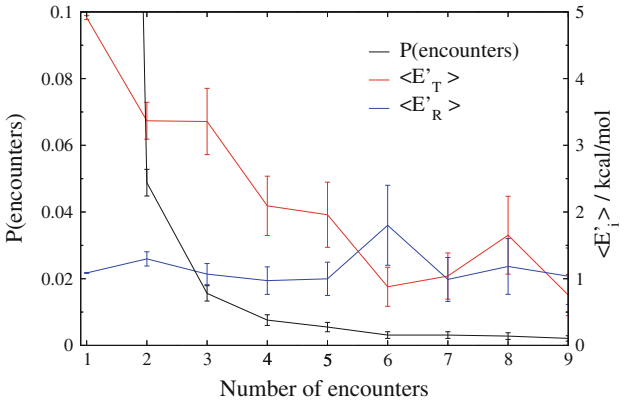

Fig. 10 Probability distribution of the number of encounters of OH with the F-SAM (*left axis*) and final average translational and rotational energy as a function of the number of gas/surface encounters in collisions of OH ($N = 5$) with fluorinated SAM surfaces at $E_{coll} = 12.8$ kcal/mol and normal incidence. The probability of 1 encounter is 0.9

OH. A second conclusion is that the initial rotational state of OH does not influence the scattering angle, as there is substantial overlap in the distributions shown in Fig. 8.

To examine whether there is a correlation between the final OH scattering angle and the extent of gas/surface energy transfer, we have calculated the final translational and rotational energy of OH as a function of its desorption angle. Figure 9 shows how the average final translational and rotational energies depend on the polar scattering angle of the desorbing OH. The figure indicates that OH desorbing near parallel to the surface has a larger translational energy than OH desorbing near normal to the surface. An increase in the translational energy with deflection angle is expected and has been seen before in various gas/organic surface detailed calculations, including Ar scattering from F-SAMs at hyperthermal energies [37], and CO scattering from CF_3-terminated SAMs [20]. Such trend is also predicted by a binary collision model in which both the projectile and surface are structureless particles with a given mass, which in the case of the surface is not well defined [38]. In the next section, we present a mechanistic analysis of the collisions to further establish whether simple models could capture the dynamics of OH + F-SAM collisions.

Counter to the trend just analyzed for final translational energy, there is little to no correlation between final rotational energy and scattering angle. The differing trends in final translational and rotational energies suggest that the mechanisms controlling whether OH retains a larger fraction of its initial collision energy are not necessarily connected to an increased rotation in OH, and this is consistent with the correlation between final OH rotation and translation seen in Fig. 7.

3.4 Mechanism

An attractive feature of atomistic molecular dynamics simulations is that they enable one to probe the microscopic mechanism of collisions. Via examination of the coordinates and momenta throughout a trajectory, the behavior a molecule during collision can be deciphered, which adds a layer of understanding to gas/surface dynamics phenomenology.

In this work, we analyze the number of encounters of the hydroxyl radical with the surface by monitoring the number of times during a trajectory that OH's center-of-mass coordinate in the surface normal direction experiences a minimum. Trajectories in which only one minimum is found correspond to collisions in which OH encounters the surface only once. Analysis of trajectories started with OH in various rotational states reveals that approximately 90% of collisions only experience one encounter with the surface, regardless of the initial rotational state. These results

clearly indicate that the mechanism of the collisions is mostly direct, i.e., the hydroxyl radical does not have a large tendency to become trapped on the surface. In the rest of trajectories, OH collides with the surface more than once, but the probability of long trapping is vanishingly small. On average, in less than 1 in 200 trajectories does OH remain trapped on the surface for longer that our integration time cutoff (10^5 atomic time units, or 24.2 ps). The lack of substantial long trapping was anticipated while mapping the potential energy surface in Sect. 2, as relatively shallow minima afford only weak attraction between OH and the surface. In addition, the rigid character of fluorinated alkane chains inhibits efficient accommodation of OH.

Even if most of the OH recoils from the surface after just one collision, it is still interesting to analyze how the final energy of OH depends on the residence time on the surface for the few trajectories in which it collides more than once with the surface. To this end, we present in Fig. 10 average final translational and rotational energies of OH as a function of the number of encounters with the F-SAM. The final translational energy clearly decreases with the number of encounters with the surface. This trend parallels recent simulations of the post-reaction dynamics of HF on alkanethiol SAM surfaces formed by hydrogen abstraction by incoming F atoms [36]. It also is consistent with the results of rare gas scattering from SAMs [18]. On the other hand, even if the statistics are poor due to the low number of trajectories that collide more than once with the surface, one cannot conclude that the number of encounters with the surface has a large effect on the amount of final rotational energy of OH. This seems to be a new paradigm, as it does not follow the results of the dynamics of HF on alkanethiol SAMs, where it was reported that the larger the number of encounters of the gas with the surface, the smaller the amount of rotational energy present in the gas after desorption [36]. A difference between the OH/F-SAM system studied in this work and the HF/H-SAM system of Ref. [36] is that in this work, there is a significant mass mismatch between the gas and the surface groups it interacts with that is not as remarkable in the case of HF interacting with CH_3-terminated SAMs. H-SAM surfaces can move laterally with more ease than F-SAMs to accommodate a gas species and efficiently absorb its rotational energy. In addition, the residence time of HF on a H-SAM surface at the conditions studied is substantially longer than that of OH on the F-SAM of this work, and this likely enables enhanced quenching of the gas rotational angular momentum by the surface. Given the intriguing trend of gas rotation with residence time on a surface unveiled in this work, in the future, it will be interesting to examine how rotational energy is transferred by a trapped species to a surface as a function of parameters such as gas and surface masses and the strength of gas/surface interactions.

4 Concluding remarks

Recent experiments on the dynamics of OH scattering from organic surfaces have motivated the detailed theoretical study presented in this work. In order to model the interfacial scattering process with confidence via atomistic molecular dynamics simulations, we have developed gas/surface potential energy surfaces based on extensive and high-accuracy ab initio calculations. These electronic structure calculations have various complications, including the fact that OH is a non-symmetrical molecule and thus mapping the entire potential energy surface is more laborious than otherwise and that OH is an open-shell species, which in this case requires one to consider two potential energy surfaces.

Derivation of pairwise analytic potentials to model the OH/fluorinated surface interaction has enabled us to propagate a few thousand trajectories of OH collisions with F-SAMs at initial conditions pertinent to the experiment. After learning that the surface density seems to play a minor role on the dynamics of the collisions, we have investigated how the product properties depend on the initial rotational state of OH. Such studies have provided the possibility to compare calculated post-collision OH rotational distributions with experiment, with which we have verified the suitability of our model. Investigation of the extent of gas/surface energy transfer indicates that some modest amount of the initial collision energy is transferred to OH rotational energy and that if OH is initially rotationally excited, there is a decrease in the amount of energy transferred to the surface.

OH desorbs from the surface in a wide range of angles, and while larger deflection angles are correlated with OH that recoils faster from the surface, the amount of rotational angular momentum is essentially independent of the angle of desorption. In addition, detailed studies of the microscopic mechanism of the collisions reveal that in most of the trajectories, there is only one collision between the gas and the surface. In trajectories where OH has the opportunity to collide a few times with the surface, a decided decrease in OH's final translational energy is appreciated. This trend contrasts sharply with the apparent resilience of OH's rotational energy to be transferred to the surface.

Acknowledgments This work has been supported by NSF Grant No. CHE-0547543 and AFOSR Grant No. FA9550-06-1-0165. D.T. is a Cottrell Scholar of Research Corporation. Computational resources have been provided by NSF Grant No. CHE-0741927. The authors would also like to thank Ken McKendrick (Heriot-Watt University) for supplying raw experimental data and valuable advice in their interpretation.

References

1. Finlayson-Pitts BJ, Pitts JN Jr (2000) Chemistry of the upper and lower atmosphere: theory, experiments, and applications. Academic Press, San Diego
2. Duce RA, Mohnen VA, Zimmerman PR, Grosjean D, Cautreels W, Chatfield R, Jaenicke R, Ogren JA, Pellizzari ED, Wallace GT (1983) Organic material in the global troposphere. Rev Geophys 21(4):921–952
3. Ellison GB, Tuck AF, Vaida V (1999) Atmospheric processing of organic aerosols. J Geophys Res Atmos 104(D9):11633–11641
4. Montzka SA, Krol M, Dlugokencky E, Hall B, Jockel P, Lelieveld J (2011) Small interannual variability of global atmospheric hydroxyl. Science 331(6013)
5. Love JC, Estroff LA, Kriebel JK, Nuzzo RG, Whitesides GM (2005) Self-assembled monolayers of thiolates on metals as a form of nanotechnology. Chem Rev 105(4):1103–1169
6. D'Andrea TM, Zhang X, Jochnowitz EB, Lindeman TG, Simpson C, David DE, Curtiss TJ, Morris JR, Ellison GB (2008) Oxidation of organic films by beams of hydroxyl radicals. J Phys Chem B 112(2):535–544
7. Fiegland LR, Saint Fleur MM, Morris JR (2005) Reactions of C=C-terminated self-assembled monolayers with gas-phase ozone. Langmuir 21(7):2660–2661
8. Ringeisen BR, Muenter AH, Nathanson GM (2002) Collisions of HCl, DCl, and HBr with liquid glycerol: Gas uptake, D → H exchange, and solution thermodynamics. J Phys Chem B 106(19):4988–4998
9. Zhang JM, Garton DJ, Minton TK (2002) Reactive and inelastic scattering dynamics of hyperthermal oxygen atoms on a saturated hydrocarbon surface. J Chem Phys 117(13):6239–6251
10. Wu BH, Zhang JM, Minton TK, McKendrick KG, Slattery JM, Yockel S, Schatz GC (2010) Scattering dynamics of hyperthermal oxygen atoms on ionic liquid surfaces: emim NTf2 and C(12)mim NTf2. J Phys Chem C 114(9):4015–4027
11. Zolot AM, Dagdigian PJ, Nesbitt DJ (2008) Quantum-state resolved reactive scattering at the gas-liquid interface: F plus squalane (C30H62) dynamics via high-resolution infrared absorption of nascent HF (v,J). J Chem Phys 129(19):194705
12. Kohler SPK, Allan M, Costen ML, McKendrick KG (2006) Direct gas-liquid interfacial dynamics: the reaction between O(P-3) and a liquid hydrocarbon. J Phys Chem B 110(6):2771–2776
13. Waring C, Bagot PAJ, Slattery JM, Costen ML, McKendrick KG (2010) O(P-3) atoms as a probe of surface ordering in 1-alkyl-3-methylimidazolium-based ionic liquids. J Phys Chem Lett 1(1):429–433
14. Bagot PAJ, Waring C, Costen ML, McKendrick KG (2008) Dynamics of inelastic scattering of OH radicals from reactive and inert liquid surfaces. J Phys Chem C 112(29):10868–10877
15. Waring C, King KL, Bagot PAJ, Costen ML, McKendrick KG (2011) Collision dynamics and reactive uptake of OH radicals at liquid surfaces of atmospheric interest. Phys Chem Chem Phys 13(18):8457–8469
16. Bosio SBM, Hase WL (1997) Energy transfer in rare gas collisions with self-assembled monolayers. J Chem Phys 107(22):9677–9686
17. Day BS, Morris JR, Alexander WA, Troya D (2006) Theoretical study of the effect of surface density on the dynamics of Ar plus alkanethiolate self-assembled monolayer collisions. J Phys Chem A 110(4):1319–1326
18. Alexander WA, Day BS, Moore HJ, Lee TR, Morris JR, Troya D (2008) Experimental and theoretical studies of the effect of mass on the dynamics of gas/organic-surface energy transfer. J Chem Phys 128(1):014713:1–014713:11
19. Nogueira JJ, Vazquez SA, Mazyar OA, Hase WL, Perkins BG, Nesbitt DJ, Martinez-Nunez E (2009) Dynamics of CO_2 scattering off a perfluorinated self-assembled monolayer. Influence of the incident collision energy, mass effects, and use of different surface models. J Phys Chem A 113(16):3850–3865
20. Alexander WA, Morris JR, Troya D (2009) Experimental and theoretical study of CO collisions with CH3- and CF3-terminated self-assembled monolayers. J Chem Phys 130(8):084702
21. Alexander WA, Troya D (2011) Theoretical study of the dynamics of collisions between HCl and omega-hydroxylated alkanethiol self-assembled monolayers. J Phys Chem C 115(5):2273–2283
22. Jorgensen WL, Maxwell DS, Tirado-Rives J (1996) Development and testing of the OPLS all-atom force field on conformational energetics and properties of organic liquids. J Am Chem Soc 117:11225–11236
23. Allinger NL, Yuh YH, Lii J-H (1989) Molecular mechanics. The MM3 force field for hydrocarbons. 1″. J Am Chem Soc 111:8551–8556
24. http://webbook.nist.gov
25. Day SB, Morris JR, Troya D (2005) Classical trajectory study of collisions of Ar with alkanethiolate self-assembled monolayers: potential-energy surface effects on dynamics. J Chem Phys 122(21):214712
26. Alexander WA, Troya D (2006) Theoretical study of the Ar–, Kr–, and Xe–CH4, –CF4 intermolecular potential-energy surfaces. J Phys Chem A 110(37):10834–10843
27. East ALL, Allen WD (1993) The heat of formation of NCO. J Chem Phys 99(6):4638–4650
28. Alexander MH (1982) Rotationally inelastic collisions between a diatomic molecule in a2Π electronic state and a structureless target *J*. Chem Phys 76:5974–5988
29. Scharfenberg L, Klos J, Dagdigian PJ, Alexander MH, Meijer G, van de Meerakker SYT (2010) State-to-state inelastic scattering of Stark-decelerated OH radicals with Ar atoms. Phys Chem Chem Phys 12(36):10660–10670
30. Aoiz FJ, Verdasco JE, Herrero VJ, Rabanos VS, Alexander MA (2003) Attractive and repulsive interactions in the inelastic scattering of NO by Ar: a comparison between classical trajectory and close-coupling quantum mechanical results. J Chem Phys 119(12):5860–5866
31. Perkins BG, Nesbitt DJ (2008) Stereodynamics in state-resolved scattering at the gas–liquid interface. Proc Natl Acad Sci USA 105(35):12684–12689
32. Camillone N, Chidsey CED, Eisenberger P, Fenter P, Li J, Liang KS, Liu GY, Scoles G (1993) Structural defects in self-assembled organic monolayers via combined atomic-beam and X-ray-diffraction. J Chem Phys 99(1):744–747
33. Liu GY, Fenter P, Chidsey CED, Ogletree DF, Eisenberger P, Salmeron M (1994) An unexpected packing of fluorinated n-alkane thiols on Au(111): a combined atomic force microscopy and x-ray diffraction study. J Chem Phys 101:4301–4306
34. Klos J, Aoiz FJ, Cireasa R, ter Meulen JJ (2004) Rotationally inelastic scattering of OH((2)Pi) by HCl((1)Sigma). Comparison of experiment and theory. Phys Chem Chem Phys 6(21):4968–4974
35. Day BS, Morris JR (2005) Packing density and structure effects on energy-transfer dynamics in argon collisions with organic monolayers. J Chem Phys 122(23):234714
36. Layfield JP, Troya D (2010) Theoretical study of the dynamics of F plus alkanethiol self-assembled monolayer hydrogen-abstraction reactions. J Chem Phys 132(13):134307
37. Tasic U, Troya D (2008) Theoretical study of the dynamics of hyperthermal collisions of Ar with a fluorinated alkanethiolate self-assembled monolayer. Phys Chem Chem Phys 10(37):5776–5786
38. Lahaye R, Kang H (2001) Energy exchange in structure scattering: a molecular dynamics study for Cs+ from Pt(111). Surf Sci 490(3):327–335